Since January 2020 Elsevier has created a COVID-19 resource centre with free information in English and Mandarin on the novel coronavirus COVID-19. The COVID-19 resource centre is hosted on Elsevier Connect, the company's public news and information website.

Journal of Molecular Structure 1228 (2021) 129454

Contents lists available at ScienceDirect

Journal of Molecular Structure

journal homepage: www.elsevier.com/locate/molstr

Synthesis, anti-bacterial evaluation, DFT study and molecular docking as a potential 3-chymotrypsin-like protease (3CLpro) of SARS-CoV-2 inhibitors of a novel Schiff bases

Ahmed S.M. Al-Janabi[a], Amin O. Elzupir[b], Tarek A. Yousef[c,d,*]

[a] Department of Biochemistry, College of Veterinary Medicine, Tikrit University, Tikrit, Iraq
[b] Imam Mohammad Ibn Saud Islamic University (IMSIU), College of Science, Deanship of Scientific Research, Riyadh, KSA
[c] Department of Chemistry, Science College, Imam Mohammad Ibn Saud Islamic University, (IMSIU), Riyadh, KSA, P.O. Box 90950, Riyadh 11623, Saudi Arabia
[d] Toxic and Narcotic drug, Forensic Medicine Department, Mansoura Laboratory, Medicolegal organization, Ministry of Justice, Egypt

ARTICLE INFO

Article history:
Received 29 August 2020
Revised 3 October 2020
Accepted 13 October 2020
Available online 17 October 2020

Keywords:
COVID 19
DFT calculations
Schiff bases
Molecular docking

ABSTRACT

New Schiff bases {N'-(phenyl(pyridin-2-yl)methylene) isonicotinohydrazide (L^1H), N^1-(naphthalen-1-yl)-N^2-(phenyl(pyridin-2-yl) methylidene) ethane-1,2-diamine (L^2H), N-(6-chlorobenzo[d]thiazol-2-yl)-1-phenyl-1-(pyridin-2-yl) methanimine (L^3H)}were synthesized by reaction of 2-benzoylpyridine with different amines (2-amino-6-chlorobenzothiazole, isonicotinohydrazide and N^1-(naphthalen-1-yl)ethane-1,2-diamine) and characterized by ^{1}H-NMR, ^{13}C-NMR, IR mass spectroscopy and elemental analysis. The compounds were assayed by the disc diffusion method for anti-bacterial against five pathogenic bacteria species (*Staphylococcus aureus, Micrococcus luteus, Staphylococcus pyogenes, Bacillus subtilis,* and *E. coli*). All prepared Schiff bases showed good activity compared to positive control (streptomycin), Moreover the **L^3H** showed the highest activity against *S. aureus, and M. luteus* than the other compounds and streptomycin. In additional molecular docking studies with 3-chymotrypsin-like protease (3CLpro), the essential enzyme for SARS-CoV-2 proliferation. The rest of compounds have shown promising results as 3CLpro inhibitors interacting with the active sites of the enzymes. Finally, DFT 's estimated electrostatic molecular potential results were used to illustrate the molecular docking findings. The DFT calculations showed that **L^3H** has the highest dipole moment and electrophilicity index. Interestingly, **L^2H** of the largest energy gap $\Delta E = 2.49$ eV, there are several hydrophilic interactions that could facilitate the binding with the receptors. All of these parameters could be shared to significantly affect the protein sites of binding affinity with different extent.

1. Introduction

Novel coronavirus (COVID-19) has arisen as an infectious disease and spread rapidly throughout the world and is transmitted mainly through contact with contaminated saliva droplets or by nose discharge while Patients diagnosed with cough or sneeze. Human coronaviruses were first described in the mid-1960s [1, 2]. Coronaviruses belong to the Coronaviridae family, a family of single stranded enveloped- positive sense RNA viruses. In addition, the Coronaviridae family was divided into four genera: α, β, γ, and δ. Coronaviruses of ubiquitous and genera commonly infect mammals and humans while birds are primarily infected by the form and generations. That specification is in line with coronavirus phylogenetic analysis and genome structure [3]. Computational features of the novel coronavirus [4, 5] or more generally new testable theories for standard drugs involved. A virtual screening technique has recently been performed to identify the active site on the viral protease for the binding of many natural compounds by molecular docking and cell-based assays [6]. Our research group recently concentrated on determining the molecular geometry of synthesized materials by comparing the desired properties from experimental evaluation to estimated parameters from computational calculations [7].

Schiff bases have been reported to possess a wide range of biological properties such as being anti-tumor, antiviral, anti-bacterial, anti-fungal and anti-inflammatory etc. [8] Schiff bases containing N, S, and O atoms in structures show an important role in biological systems because they have unusual electronic properties [9].

2-phenylquinazoline-4(3)H-one Schiff bases are confirmed to have antiviral activity against certain strains of viruses, such as feline corona virus, influenza Viruses, and type 1 and type 2 herpes simplex viruses [10]. From published literature, the antiviral ability

* Corresponding author.
E-mail addresses: drroka78@yahoo.com, tayousef@imamu.edu.sa (T.A. Yousef).

https://doi.org/10.1016/j.molstruc.2020.129454
0022-2860/

of these Schiff bases is evident and thus further focused work will help to discover and improve new potential lead compounds to use them as drug candidates.

Recently a novel SARS-CoV-2 virus properly originated from bat was reported, cause the severe acute respiratory syndrome, known as COVID-19 [11–13]. The enzyme 3-chymotrypsin-like protease ($3CL^{pro}$) cleaves at least 11 sites on the polyproteins translated from the viral RNA of SARS-CoV-2. Thus, the compounds having ability to inhibit this enzyme can be considering as an effective therapeutic agent for COVID-19. This work describes the synthesis and spectroscopic characterization of new Schiff bases and evaluated as anti-bacterial, besides, the synthetic compounds have also been studied as 3CLpro inhibitors.

2. Experimental

2.1. Materials and methods

2-amino-6-chlorobenzothiazole, isonicotinohydrazide, N^1-(naphthalen-1-yl)ethane-1,2-diamine, 2-benzoylpyridine and solvents were obtained through Sigma-Aldrich, and used without any further purification. ^{1}H and ^{13}C NMR spectra were recorded on Bruker Avance 400 MHz NMR spectrometer in DMSO as deuterated solvent. The melting point was measured using SMP30 melting point apparatus. IR spectra were recorded on a Shimadzu FT-IR 8400 spectrophotometer using KBr discs in 400-4000 cm^{-1} range.

2.2. Preparation of Schiff bases

2.2.1. Preparation of N'-(phenyl(pyridin-2-yl)methylene) isonicotinohydrazide (L^1H)

A colorless solution of 2-benzoylpyridine (0.730 g, 3.985 mmol) in EtOH (15mL) was added to an ethanol solution of isonicotinohydrazide (0.547g, 3.985 mmol) in (20 mL) with some drops of glacial acetic acid. The mixture was refluxed for 6 h, the formed solution was filtered and left aside to cool slowly, then the dark creamy ppt. was separated and recrystallized from hot ethanol and dried under vacuum.

L^1H. Dark creamy powder. Yield: (1.16 g, 91%). M.p. 182-183°C. Anal. Calc. for $C_{18}H_{14}N_4O$, (%):C, 71.51; H, 4.67; N, 18.53. Found C, 71.69; H, 4.53; N, 18.62. IR (KBr, cm^{-1}): 3110m(NH), 3049m, 2858m, 1668(C=O), 1633s (C=N), 1554s(C=C), 1487w, 1407s, 1330s, 1135s, 995s, 844s, 744s.^{1}H NMR (δ, ppm, DMSO-d_6): δ 11.53(s, 1H, NH), 8.92(d, J = 7.2 Hz, 2H, H15,16), 8.74 (dd, J = 7.4, 2.5 Hz, 1H, H1), 8.12 (dd, J = 7.4, 1.3 Hz, 1H, H3), 7.92(d, J = 7.2 Hz, 2H, H14,17), 7.71 (d, J = 7.6 Hz, 1H, H4), 7.62 (d, J = 7.5 Hz, 1H, H2), 7.39 (m, 5H, H8-12). ^{13}C NMR (δ, ppm, DMSO-d_6): δ 169.53 (**C**=O), 161.92 (**C**6), 152.13(**C**5), 149.73(**C**1), 147.81(**C**15,16), 140.29(**C**7), 132.63(**C**3), 131.04(**C**8,12), 129.78(**C**10), 128.12(**C**9,11), 123.22 (**C**14,17), 119.39(**C**4). ESI-MS (m/z), calc. $C_{18}H_{14}N_4O$, 302.116, found, 302.117.

2.2.2. Preparation of N^1-(naphthalen-1-yl)-N^2-(phenyl(pyridin-2-yl) methylidene) ethane-1,2-diamine (L^2H)

L^2H was prepared by a similar method to that of L^1H using N^1-(naphthalen-1-yl)ethane-1,2-diamine in place of isonicotinohydrazide.

L^2H. Light brown-yellow powder. Yield: (1.20 g, 86%). M.p. 167-168°C. Anal. Calc. for $C_{24}H_{21}N_3$ (%):C, 82.02; H, 6.02; N, 11.96. Found C, 82.17; H, 6.23; N, 12.18. IR (KBr, cm^{-1}): 3131m (NH), 3087m, 2945w(C-H), 1639s (C=N), 1529s(C=C), 1452s, 1311s, 1164w, 927m, 811s, 690s, 607m. ^{1}H NMR (δ, ppm, DMSO-d_6): δ 8.72 (ddd, J = 6.7, 1.4 Hz, 1H, H2), 8.07 (ddd, J = 7.7, 1.7 Hz, 1H, H3), 7.98 (m, 4H, H2,4,14,15), 7.67 (m, 3H, H9,10,11), 7.54 (t, J = 7.7 Hz, 2H, H8,12), 7.43 (s, 1H, NH), 7.32 (d, J = 6.8 Hz, 2H, H19,22), 7.21 (d, J = 8.1 Hz, 1H, H14), 7.01(dd, J = 7.7 Hz, 2H, H20,21), 2.302 (s, 4H, NH-CH_2), 2.295 (s, 2H, CH_2C=N). ^{13}C NMR (δ, ppm, DMSO-d_6): δ 165.28 (**C**6), 154.13(**C**13), 150.29(**C**5), 148.21(**C**1), 137.30(**C**7), 135.64(**C**17), 132.639(**C**3), 130.64(**C**18), 130.22(**C**8,12), 129.50(**C**10), 127.85(**C**9,11), 126.37(**C**16,19), 126.04(**C**15,22), 123.78(**C**20,21), 120.44(**C**4), 117.04(**C**14), 21.48 (**C**H_2-N=C) 20.36 (**C**H_2-NH). ESI-MS (m/z), calc. $C_{24}H_{21}N_3$, 351.174, found, 351.176.

2.2.3. Preparation of N-(6-chlorobenzo[d]thiazol-2-yl) -1-phenyl-1-(pyridin-2-yl) methanimine (L^3H)

L^3H was prepared by a similar method to that of L^1H using 2-amino-6-chlorobenzothiazole in place of isonicotinohydrazide.

L^3H. brownish yellow powder. Yield: (0.93 g, 76%). M.p. 156-158°C. Anal. Calc. for $C_{19}H_{12}ClN_3S$, (%):C, C, 65.23; H, 3.46; N, 12.01; S, 9.16. Found C, 65.15; H, 3.28; N, 12.31; S, 9.23. IR (KBr, cm^{-1}): 3086m(CH), 1627s (C=N), 1542s(C=C), 1415s, 1315s, 1274s, 1141s, 1088s, 698s, 651m.^{1}H NMR (δ, ppm, DMSO-d_6): δ 8.80 (dd, J = 7.8, 1.7 Hz, 1H, H1), 8.12 (s, 1H, H18), 7.98 (dd, J = 7.6, 1.5 Hz, 1H, H3), 7.72(d, J = 7.4 Hz, 2H, H4), 7.68(d, J = 7.6 Hz, 1H, H2), 7.56 (m, 4H, H8,12,15,16), 7.36(m, 3H, H9-11). ^{13}C NMR (δ, ppm, DMSO-d_6): δ 171.78 (**C**13), 162.45 (**C**6), 153.40(**C**5), 148.92(**C**1), 147.81(**C**14), 141.55(**C**7), 134.07(**C**3), 133.65(**C**19), 131.73(**C**8,12), 128.96(**C**10), 128.03(**C**9,11), 126.56(15), 123.22(**C**16), 120.78(**C**18), 118.77(**C**4), 116.78(**C**17). ESI-MS (m/z), calc. $C_{19}H_{12}ClN_3S$, 349.044, found, 349.033.

2.3. Antibacterial studies

The anti-bacterial activities of the complexes were tested by agar disc diffusion method originally described by Bauer [14] against five bacteria types, *Staphylococcus* aureus, *Micrococcus luteus, Staphylococcus pyogenes, Bacillus subtilis,* and *E. coli* in (50, 100, and 200 μg) of each compound compared with streptomycin as positive control.

Minimum inhibitory concentration (MIC) of the Schiff bases were tested in in Nutrient broth for bacteria by the two-fold serial dilution method [15]. The bacterial suspension was attuned with sterile saline to a concentration of $1^{*}10^{-5}$ - 10^{-6} CFU. The tested compounds and standard control (Streptomycin) were prepared by two-fold serial dilution to obtain the essential concentrations of 200, 100, 50, 25, 12.5 and 6.25 μg/mL. The tubes were incubated in incubators at 37 °C. The MICs were recorded by visual observations after 24 h.

2.4. Optimization and molecular docking

The three-dimensional structures of the **L^1H, L^2H**, and **L^3H** were generated and optimized by Gaussian 09 program package [16] software. The crystal structure of $3CL^{pro}$ of SARS-CoV-2 was obtained from the Protein Data Bank database (PDB ID: 6Y2E). Molecular docking experiments were carried out using the AutoDock Vina tool plugin UCSF Chimera software (v 1.14), adopting the default values for the parameters, and a grid box (-16 × -24.0 × 17) Å was centered at (35, 65, 65) Å. In order to represents the real environment, water was added as a solvent, with accessible surface area of 14358.5. The predicted binding affinity score was explored utilizing the View Dock tool. The binding to active sites and images were processed by the UCSF Chimera [17–19].

3. Results and discussion

3.1. Synthesis of Schiff bases

The Schiff bases have been synthesized by condensation of 2-benzoylpyridine with 2-amino-6-chlorobenzothiazole or isonicotinohydrazide or N^1-(naphthalen-1-yl)ethane-1,2-diamine to afford a

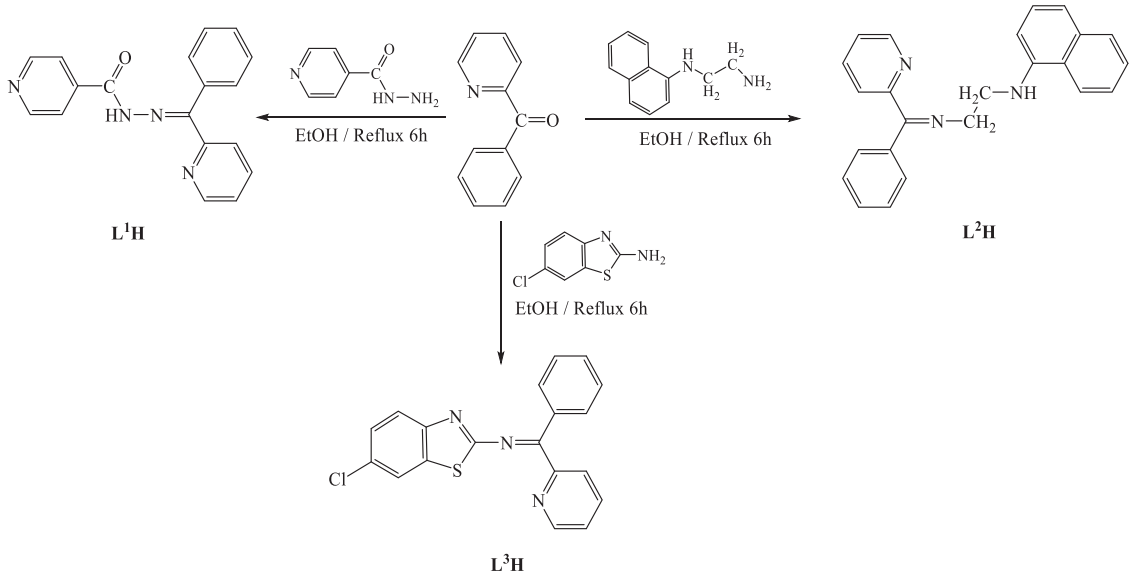

Scheme 1. Preparation of Schiff bases **L¹H, L²H** and **L³H**

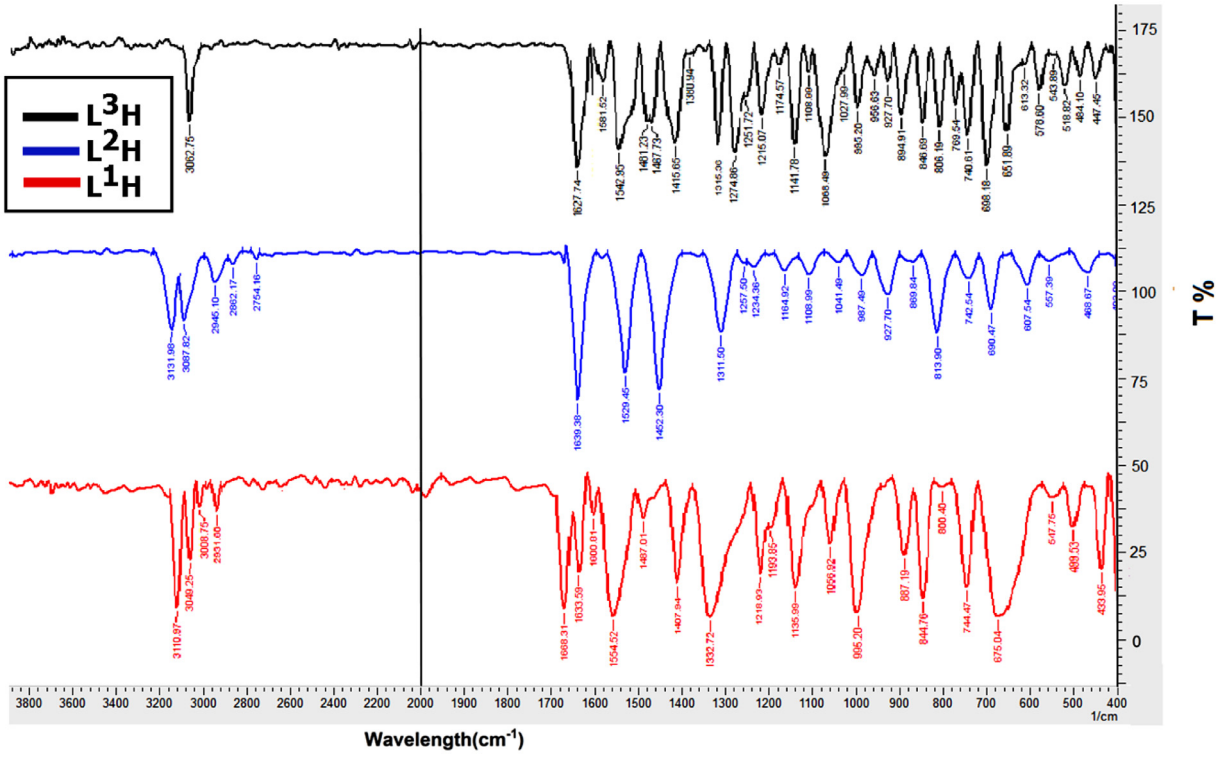

Fig. 1. IR spectra of the prepared Schiff bases

dark creamy with **L¹H**, light brown-yellow in **L²H**, and a brownish yellow with **L³H** (**Scheme 1**). The prepared Schiff bases are stable in air and soluble in EtOH, DMSO and DMF. The compounds were characterized by using elemental analysis, ^{1}H, ^{13}C NMR, and IR techniques. All attempts to get crystals suitable for X-ray diffraction studies were unsuccessful.

3.2. Characterization of Schiff bases

3.2.1. IR Spectra

The IR spectra of the prepared Schiff bases (Fig. 1) displayed a strong band within the 1627-1639 cm^{-1} range for the azomethine group υ(C=N) [20–22]. And disappeared the υ(C=O) of 2-phenylpyridine, and $\upsilon(NH_2)_{sy,\ asy}$ stretching vibration of amine, indicates the formation of the proposed compounds. The υ(C=C) vibration of the aromatic rings showed within the 1529-1554 cm^{-1} range [22]. The spectra of **L¹H** and **L²H** displayed a medium band at 3110cm^{-1} and 3131cm^{-1}assigned to the υ(N-H). And the **L¹H** spectrum appeared the υ(C=O) of isonicotine group at 1668cm^{-1} [23] Also the spectrum of **L²H** showed the stretching vibration of aliphatic group at 2945cm^{-1} [22]. Other vibrations are listed in experimental section.

3.2.2. ^{1}H and ^{13}CNMR spectra

The ^{1}H-NMR spectrum of **L¹H** in DMSO-d_6 displayed the **NH** proton at δ11.53 ppm as a singlet peak. And four doublet peaks

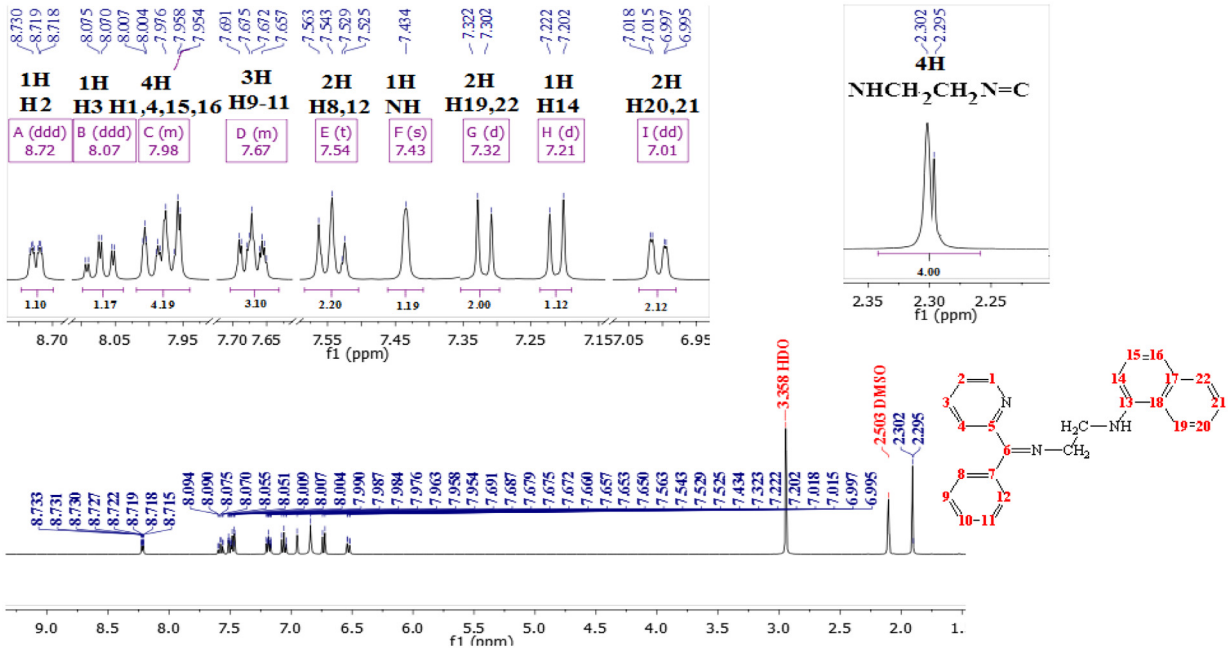

Fig. 2. ^{1}H NMR spectrum of the **L^{2}H** in DMSO-d_6

at δ8.92ppm, δ7.92ppm, δ7.71ppm and δ7.62ppm, assigned to the **H15,16, H14,17, H4**, and **H2**, corresponding to 2,1,2,1 protons respectively. Also the spectrum showed two doublet of doublets peaks at δ8.74ppm, and δ8.12ppm for the **H1** and **H3**, respectively. A multiplet peak was showed at δ7.39ppm assigned to protons in position **8-12** (phenyl ring) (**Fig. SI1, supporting information**).

The ^{1}H-NMR spectrum of **L^{2}H** (Fig 2), clearly display the phenyl protons belong to the pyridyl, phenyl and naphthyl rings. A two doublet peaks displayed at δ7.21ppm and δ7.32ppm due to a **H14** and **H19,22**, corresponding to one and two protons, respectively. And two doublet of doublet of doublets at δ8.72ppm, and δ8.07ppm for the **H2** and **H3**, respectively. Also the spectrum displayed two multiplets peaks at δ7.98ppm and δ7.67ppm, due to the protons in position (**1,4,15,16**) and (**9-11**), respectively. The protons in position **20** and **21** appeared as doublet of doublets at δ7.01ppm (J_{HH} = 7.8 Hz). And the **H8,12** showed as triplet peak at δ7.54ppm with coupling constant to the neighboring protons (J_{HH} = 7.7 Hz). The **NH** proton was showed at δ7.43 ppm as a singlet peak, whereas the methylene groups displayed as two singlet at δ2.302 and 2.295 ppm, due to the NH-C $\underline{H}_2$ and C $\underline{H}_2$N=C, respectively, corresponding to four protons.

The ^{1}H-NMR spectrum of **L^{3}H** in DMSO-d_6 showed two doublet of doublets peaks at δ8.80ppm, and δ7.98ppm for the **H1** and **H3**, respectively. And two doublet peaks at δ7.72ppm, and δ7.56ppm, due to the **H4** and **H2**, corresponding to one proton of each peak, respectively. Also the spectrum showed two multiplet peaks were showed at δ7.56ppm and δ7.36ppm due to protons in position (**8,12,15,16**) and (**9-11**). The H18 was showed as a singlet peak at δ8.12ppm (**Fig. SI 3, supporting information**).

The above results were supported by ^{13}C NMR and elemental analysis data (Fig. 3). The δC of the azomethine group ($\underline{C}$6) of the new Schiff bases appeared at δ161.92ppm, 165.28ppm, and 162.45ppm for the **L^{1}H, L^{2}H** and **L^{3}H** respectively. Whereas the C1 displayed at δ148.21ppm, 149.73ppm, and 148.92ppm, respectively. And that the methylene group of the **L^{2}H** appeared at δ21.48ppm, 20.36ppm assigned to ($\underline{C}H_2$-N=C) and ($\underline{C}H_2$-NH) respectively. The spectrum of **L^{1}H** displayed the chemical shift of carbonyl group at δ 169.53ppm. Other ^{13}C chemical shifts are listed in experimental section(**Fig. SI 2 and 4, supporting information**).

3.3. Antibacterial activity

Antibacterial activity of the Schiff bases (**L^{1}H, L^{2}H** and **L^{3}H**) are summarized in Table 1**.** The data were obtained against five types of the pathogen bacteria (*Staphylococcus aureus, Micrococcus luteus, Staphylococcus pyogenes, Bacillus subtilis,* and *Escherichia coli* in (50, 100, and 200 μg/Disc) of each compound compared with streptomycin as positive control. The diameter of the inhibitory zone (DIZ) was compared to that of streptomycin, which is the positive control. The compounds displayed good activity against the bacteria. The Schiff base **L^{3}H** is more active for the tested bacteria compared with other Schiff bases (**L^{1}H**, and **L^{2}H**), whereas the L^{2}**H**, exhibits less activity against all the tested bacteria. Also designate the increasing concentration of Schiff bases from 50 to 200 μg/disc, the inhibition effect is increased.

The MICs are given in Table 2. Schiff base **L^{3}H** displayed the highest effective against the tested bacteria *S. aureus, M. luteus, S. pyogenes, B. subtilis* with MIC values of 6.25, 25, 25, and 25μg/mL, respectively, but less active against *E. coli*, with MIC value 100μg/mL. The antibacterial activity of **L^{3}H** is more active than the other Schiff bases (**L^{1}H**, and **L^{2}H**), suggesting the **L^{3}H** compound has a (Cl and S) atoms in the structure, these atoms possibly via enhanced membrane transport into the cell or some other mode of action [24, 25].

3.4. Theoretical studies

3.4.1. DFT calculations studies

At B3LYP 6-311G (d,p) basis set, the theoretical DFT calculations were carried out in gas phase by DFT method. The results of the theoretical DFT calculations for all the compounds under investigation (Figs 4–6) showed the non-planarity. Table 3 summarizes the approximate calculations of DFT for Electronic Energy, Heat Capacity, Entropy (S), Thermal Energy, polarizability, and dipole moment of **L^{1}H, L^{2}H**, and **L^{3}H**.

DFT calculated data showed that the **L^{1}H, L^{2}H**, and **L^{3}H** dipole moment are in the order of **L^{2}H** < **L^{3}H** < **L^{1}H.** The high dipole moment **L^{1}H** may demonstrate their binding pose within a specific target protein and its results from the predicted binding affin-

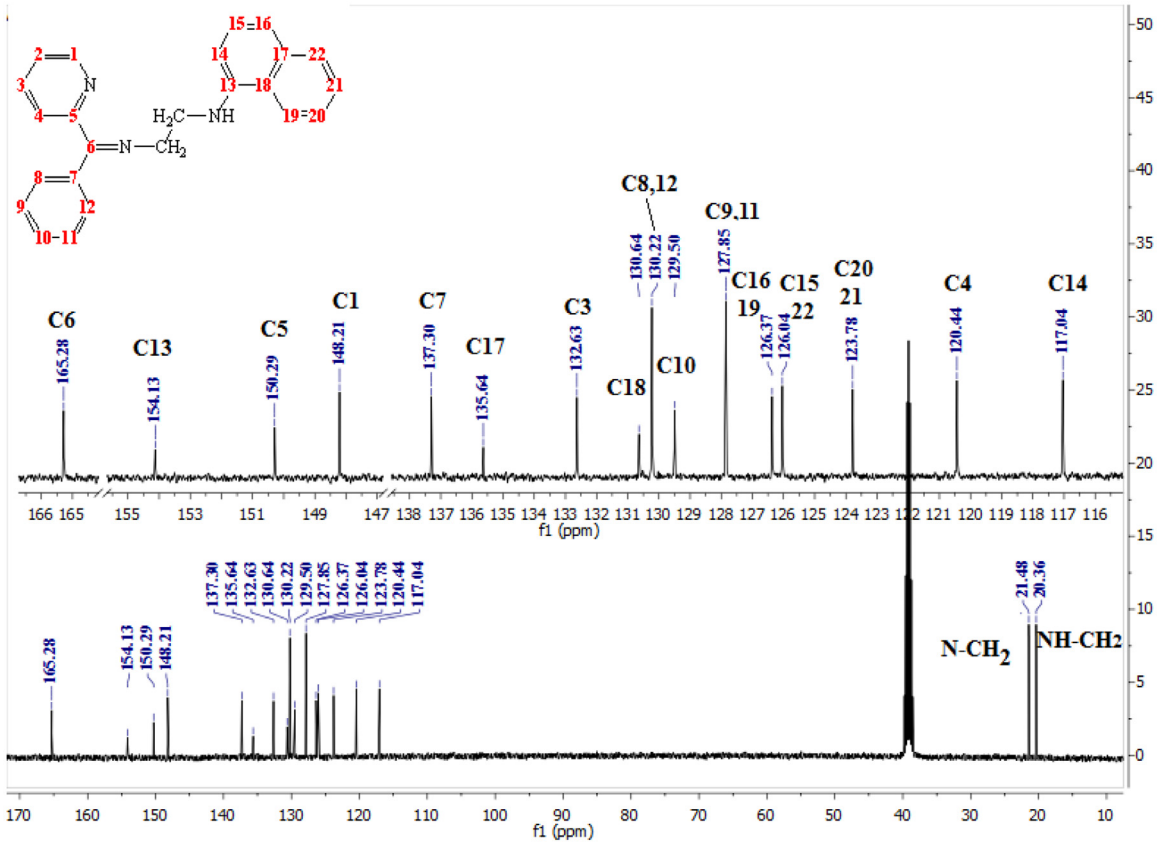

Fig. 3. ^{13}C NMR spectrum of the **L^{2}H** in DMSO-d_6

Table 1
Antibacterial activity (diameter of inhibition zone (cm)) of Schiff bases against five four different bacterial species

Comp.	Conc. μg/disc	**Micrococcus luteus**	**Staphylococcus aureus**	**Staphylococcus pyogenes**	**Bacillus subtilis**	**Escherichia coli**
L^{1}H	**50**	**9**	**12**	**11**	**8**	**10**
	100	**14**	**15**	**14**	**12**	**13**
	200	**19**	**19**	**18**	**17**	**17**
L^{2}H	**50**	**9**	**8**	**10**	**9**	**9**
	100	**13**	**12**	**12**	**12**	**11**
	200	**16**	**17**	**15**	**17**	**14**
L^{3}H	**50**	**12**	**14**	**13**	**10**	**11**
	100	**16**	**20**	**17**	**15**	**14**
	200	**19**	**24**	**18**	**19**	**18**
Streptomycin	**100**	**22**	**19**	**21**	**19**	**23**

Table 2
Minimum inhibitory concentration (MIC) in (μg/mL) of Schiff bases.

Compounds	Micrococcus luteus	Staphylococcus aureus	Staphylococcus pyogenes	Bacillus subtilis	Escherichia coli
L^{1}H	50	25	100	50	100
L^{2}H	25	50	50	100	50
L^{3}H	25	12.5	25	25	100
Streptomycin	12.5	3.12	6.25	12.5	6.25

Table 3
Electronic Energy (Hartree/Particle), Heat Capacity (Cv), Entropy (S) (cal/mol-kelvin), Thermal Energy polarizability α (a.u.), and dipole moment (Debye) of **L^{1}H, L^{2}H,** and **L^{3}H**

Parameter	L^{1}H	L^{2}H	L^{3}H
Electronic Energy	-988.49	-1091.40	-1745.44
Total Dipole Moment	7.99	2.59	3.33
Polarizability (α)	235.49	285.79	268.28
E (Thermal)	192.294	261.24	69.58
Heat Capacity (Cv)	69.839	86.79	67.89
Entropy (S)	142.655	166.53	134.04

ity to be discussed in the next molecular docking section. The polarizability of the materials depends on how a charge approach influences the resistance of the molecular system electron cloud. Additionally, it depends on the nature of the compounds and the scale of the molecular structure. Large-sized molecules are more polarizable compounds. **L^{1}H** is the smallest in size and has the least polarizability (235.49 a.u.), but **L^{2}H** with the greatest complexity is expected to have the greatest polarizability, (285.79 a.u.). Ultimately, heat capacity is the one with the most complex set of concepts and the richest set of consequences for protein folding and binding, of all the major thermodynamic variables cal-

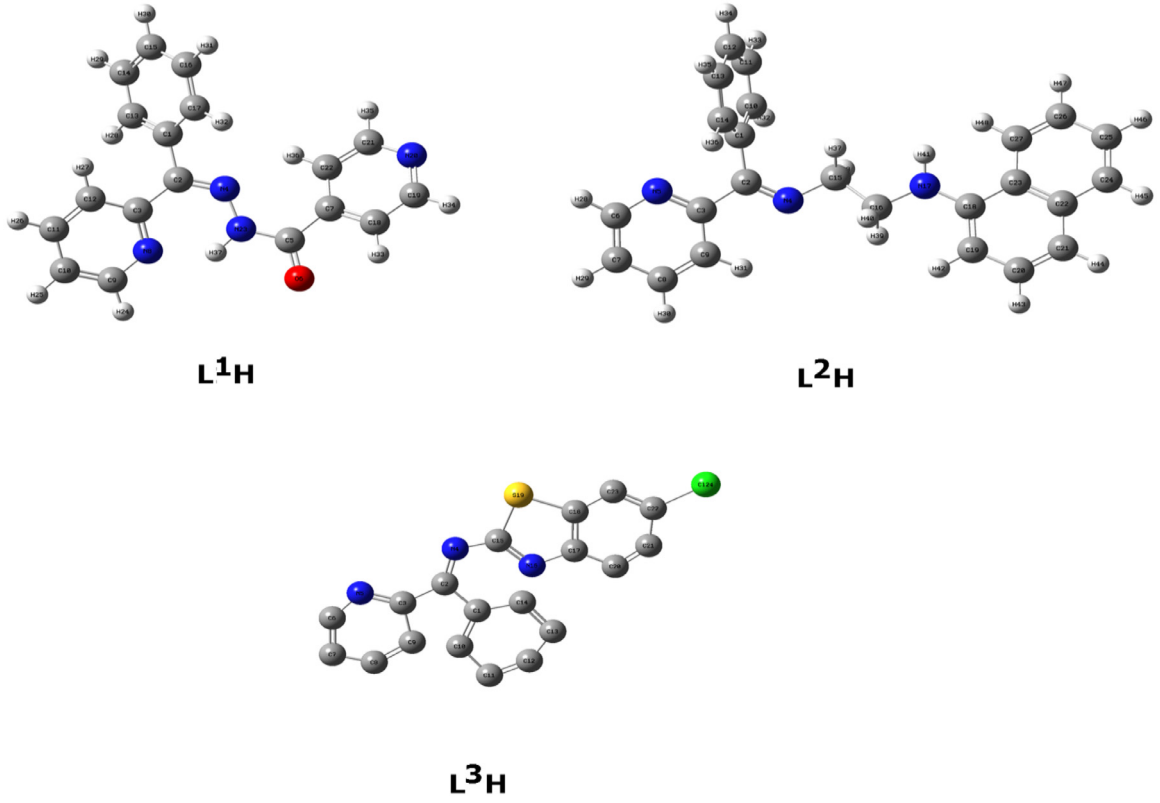

Fig. 4. Optimized geometrical structures of L^1H, L^2H, and L^3H with atomic numbering.

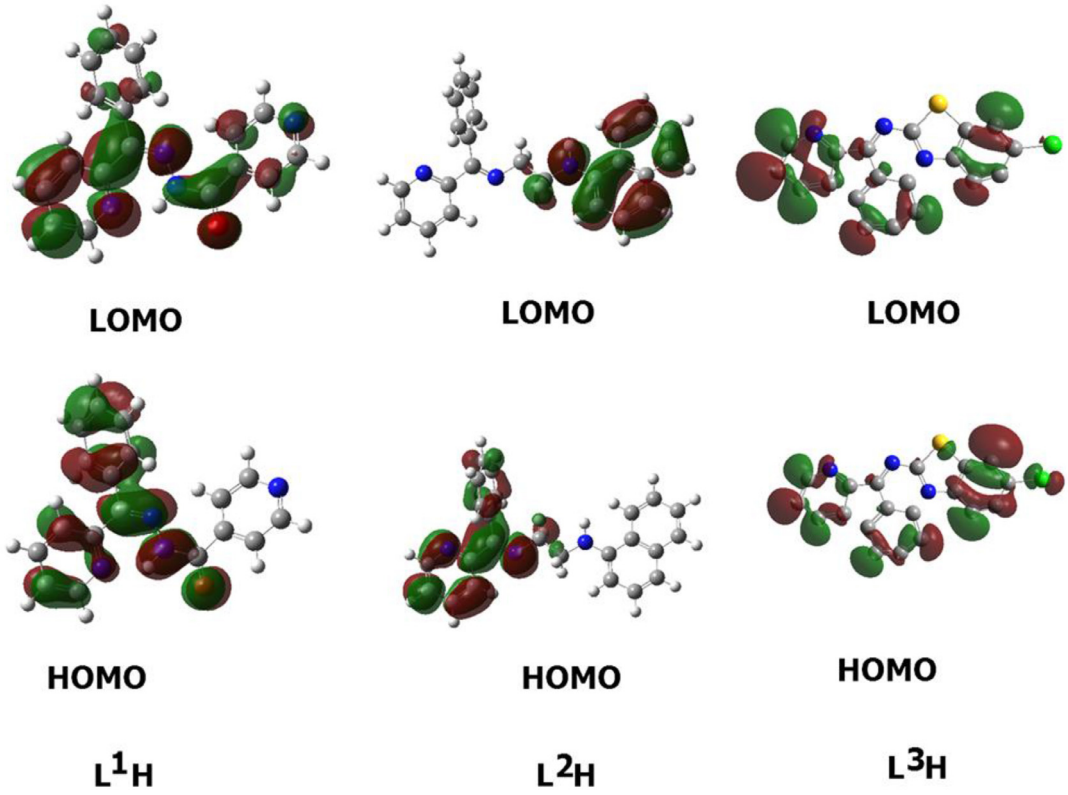

Fig. 5. HOMO and LUMO plots of the L^1H, L^2H, and L^3H compounds

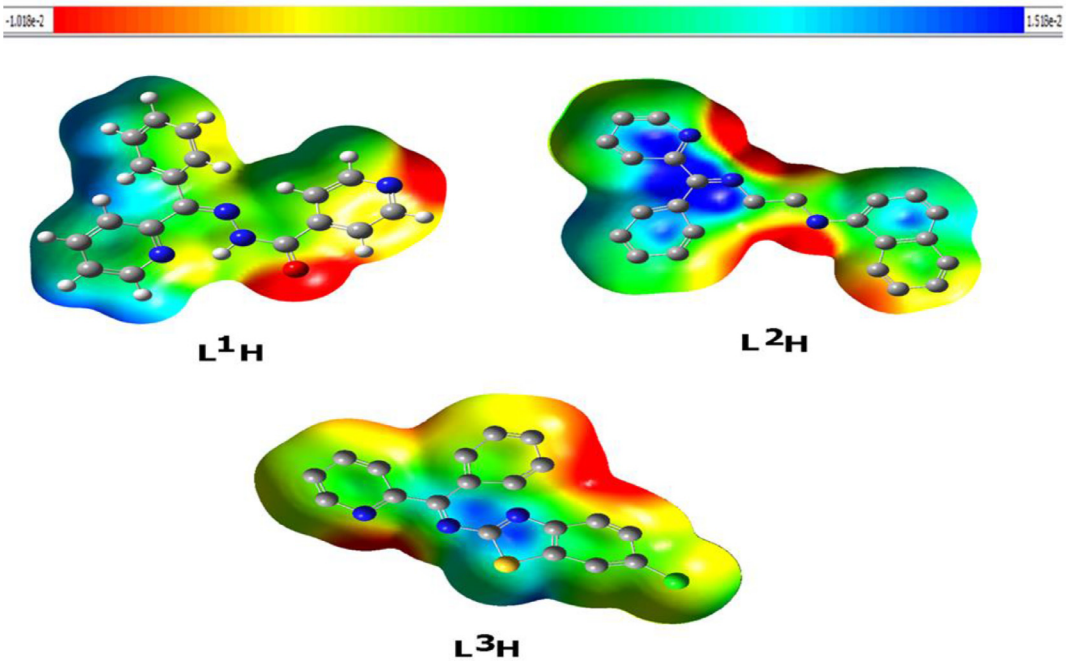

Fig. 6. Molecular electrostatic potentials (MEP) of the **L^1H, L^2H, and L^3H** compounds

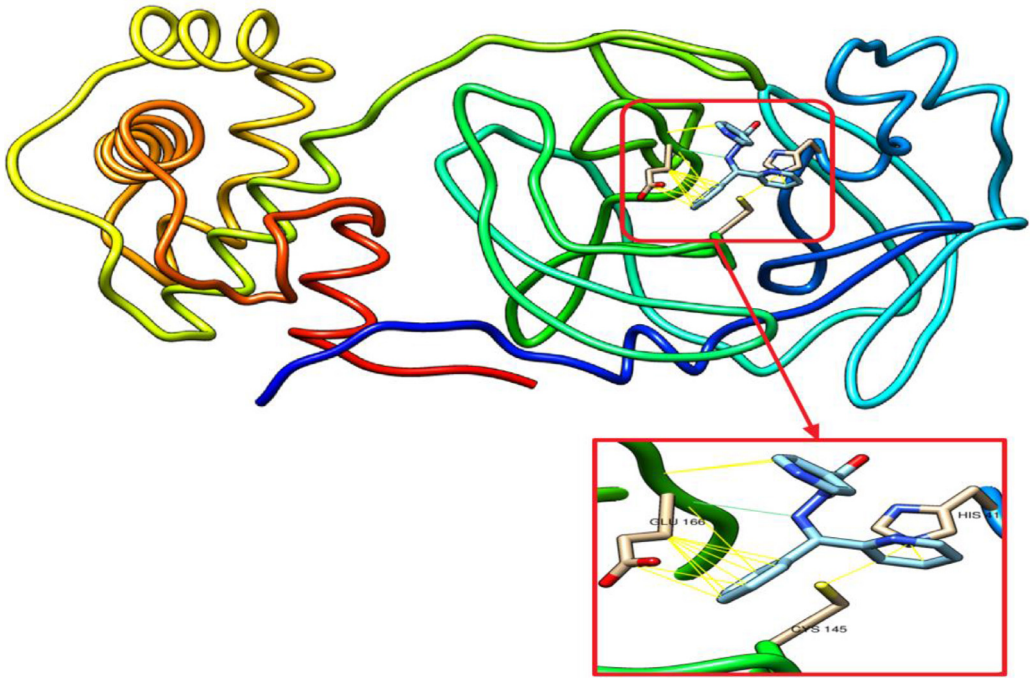

Fig. 7. **L^1H** docked with 3-chymotrypsin-like protease ($3CL^{pro}$) of SARS-CoV-2. Hydrocarbon skeleton of **L^1H** is cyan, nitrogen atoms are blue, oxygens red. Below, different side of view of magnified images of its contact sites to HIS^{41}, CYS^{145} and GLU^{166}.

culated for proteins. It gives entropy and enthalpy a temperature dependency which will alter their signs and determine which of them will dominate. The heat capacity order is as follows: **L^3H** < **L^1H** < **L^2H**. The unfolding protein typically has a positive Cp, which results in optimum stability and often cold denaturation [26].

3.4.2. Frontier molecular orbitals

The frontier molecular orbitals (FMO) can provide objective qualitative information about the HOMO electrons being susceptible to transfer to the LUMO. In addition, HOMO and LUMO are very useful quantum chemical parameters to assess the molecules' reactivity and are used to measure other parameters, such as the descriptors for chemical reactivity. The energies of the studied compounds' HOMOs and LUMOs were measured using DFT method at the base set of B3LYP 6-311 G (d, p) and are tabled in Table 4. The isodensity surface plots of HOMO and LUMO for **L^1H, L^2H,** and **L^3H** are shown in Fig. 5.

The results of the FMOs energy analysis revealed that the energies of HOMOs of **L^3H** is higher compared with **L^1H** and **L^2H**. However, the destabilization of the LUMO level is found to be higher in **L^3H** than the others. Consequently, the energy gap is in the order of **L^1H** < **L^3H** < **L^2H**.

Table 4
Calculated EHOMO (EH), ELUMO (EL), energy band gap (EH – EL), chemical potential (μ), electronegativity (χ), global hardness (η), global softness (S), global electrophilicity index (ω) and softness (σ) for **L^1H, L^2H,** and **L^3H**.

Comp.	EH / eV	EL / eV	(EL-EH) /Ev	χ / eV	μ / eV	η / eV	S / eV^{-1}	ω / eV	σ / eV^{-1}
L^1H	-6.6	-6.16	0.44	6.38	-6.38	0.22	0.11	92.51	2.27
L^2H	-7.32	-4.83	2.49	6.075	-3.78	1.245	0.6225	5.74	0.40
L^3H	-5.39	-4.72	0.67	5.055	-1.55	0.335	0.1675	3.56	1.49

Recently, many reports showed that the FMOs have to be taken into consideration in investigation of the structure activity relationships [27–29]. The FMOs theory showed that the energy level of the HOMO and the LUMO are the most significant aspects that impact the bioactivities of small structural drugs. Mainly HOMOs that offer electrons, however, the LUMOs accept electrons. Obviously, the level of energy of HOMOs are different for all studied compounds. **L^3H** showed the most lying HOMO than the other compounds and consequently it could be a better electron donor drug. Interestingly, **L^2H** of the largest energy gap $\Delta E = 2.49$ eV, there are several hydrophilic interactions that could facilitate the binding with the receptors. This suggests that such hydrophilic interactions considerably impact the binding affinity of such small drugs to the receptors. The HOMO of a certain drug and the LUMO with the adjacent residues could share the orbital interactions during the binding process.

3.4.3. Chemical reactivity descriptors

Calculations, such as the energy of the highest occupied molecular orbital, EHOMO, energy of the lowest unoccupied molecular orbital, ELUMO, obtain quantium chemical parameters of organic compounds. Additional parameters, such as separation energies (ΔE), absolute electro-negativities (v), chemical potentials (Pi), absolute hardness (g), absolute softness (r), global electrophilicity (x), global and softness (S) were calculated by Eqs. (1–3) [30, 31].

$$\chi = -1/2(E_{LUMO} + E_{HOMO}) \quad (1)$$

$$\mu = -\chi = 1/2(E_{LUMO} + E_{HOMO}) \quad (2)$$

$$\eta = 1/2(E_{LUMO} - E_{HOMO}) \quad (3)$$

$$S = 1/2\eta \quad (4)$$

$$\omega = \mu^2/2\eta \quad (5)$$

The inverse value of the global hardness is designed as the softness (σ) as follow:

$$\sigma = 1/\eta \quad (6)$$

3.4.5. Molecular electrostatic potential (MEP)

The molecular electrostatic potential (MEP) is important to quantify in order to validate the evidence regarding the reactivity of the compounds studied as inhibitors. Even though the MEP provides an indication of the molecular size and shape of both the positive, negative and neutral electrostatic potential. This may be a method for predicting relationships of physicochemical properties with the molecular structure of the drugs being investigated. In addition, the electrostatic molecular potential is a valuable method for estimating drug reactivity against electrophilic and nucleophilic attacks.

Under the same base sets, the molecular electrostatic potential of the **L^1H, L^2H**, and **L^3H** is determined using the same process and is seen in Fig. 6. The maximum negative area within the MEP is the chosen electrophilic attack sites, indicated as red color. So, the negatively charged sites, and the reverse satiation for the blue regions, should draw an attacking electrophile. It is apparent that the molecular size and shape as well as the orientation of the negative, positive, and neutral electrostatic potential differed by product due to the type of atoms and their electronic existence. The difference in mapping the electrostatic potential around the compound may be primarily responsible for variation of its binding receptor affinities.

Table 5
The Mulliken atomic charges of **L^1H, L^2H,** and **L^3H**.

L^1H			L^2H			L^3H		
1	C	-0.11122	1	C	-0.01515	1	C	-0.2013
2	C	0.106601	2	C	0.003903	2	C	0.280357
3	C	0.134528	3	C	0.130135	3	C	0.068197
4	N	-0.16705	4	N	-0.26368	4	N	-0.35022
5	C	0.511645	5	N	-0.33433	5	N	-0.3283
6	O	-0.39734	6	C	0.205425	6	C	0.106955
7	C	-0.09115	7	C	-0.02753	7	C	0.039048
8	N	-0.4852	8	C	0.005259	8	C	0.026534
9	C	0.051185	9	C	0.051085	9	C	0.060093
10	C	-0.20289	10	C	0.067703	10	C	-0.03639
11	C	-0.09894	11	C	-0.03372	11	C	0.026019
12	C	-0.09495	12	C	0.028768	12	C	-0.02273
13	C	-0.1082	13	C	-0.07759	13	C	0.096392
14	C	-0.16576	14	C	0.106634	14	C	0.137059
15	C	-0.12612	15	C	0.123458	15	C	0.177593
16	C	-0.16461	16	C	0.192665	16	N	-0.65011
17	C	-0.08972	17	N	-0.38104	17	C	0.285513
18	C	-0.17746	18	C	0.119451	18	C	-0.48668
19	C	-0.00069	19	C	0.056393	19	S	0.552361
20	N	-0.33001	20	C	-0.01049	20	C	0.167863
21	C	-0.03167	21	C	0.034302	21	C	0.035451
22	C	-0.08019	22	C	-0.05817	22	C	-0.23807
23	N	-0.56129	23	C	0.008089	23	C	0.13635
			24	C	0.005574	24	Cl	0.118015
			25	C	0.000038			
			26	C	-0.01433			
			27	C	0.077149			

3.4.6. Mulliken atomic charges

The Mulliken atomic charges of the estimated compounds (**1**–**3**) were calculated the DFT using B3LYP 6-311G (d,p) at a basis set, the data were tabulated in Table 5. It showed that the C5 is the most positive and O6 have the most negative charge for **L^1H.** In case of **L^2H** it is observed that the most nucleophilic centers are N4, N5 and N17 which are the most electrophilic susceptibility positions. On the other hand, it is obvious that the nucleophilic susceptibility of the **L^2H** is recognized on C16 sites. However, N4, N5 and N16 are the most negative charges of **L^3H**, while its respective positively charged atoms are C5 and S19**.** The positively charged centers are the most susceptible sites for nucleophilic attacks i.e., electron donation. However, the most negatively charged centers are the most susceptible sites for electrophilic one **[**32**]**.

3.5. Molecular docking

The synthetic novel Schiff bases have shown a significant rule against CL^{pro}, the important enzyme for proliferation of SARS-COV-

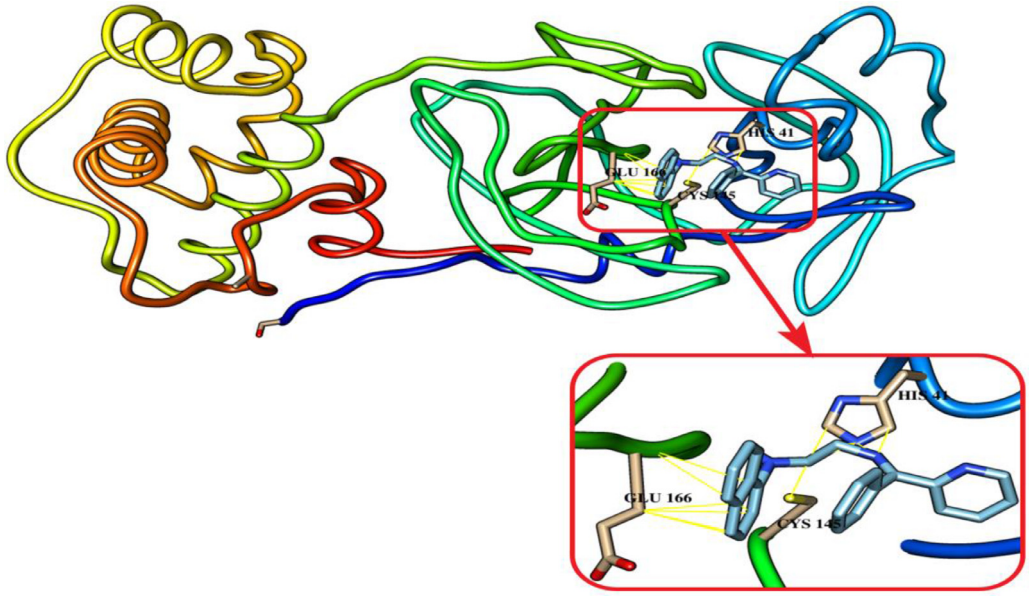

Fig. 8. **L²H** docked with 3-chymotrypsin-like protease (3CL^{pro}) of SARS-CoV-2. Hydrocarbon skeleton of **L²H** is cyan, nitrogen atoms are blue, oxygens red. Below, different side of view of magnified images of its contact sites to HIS^{41}, CYS^{145} and GLU^{166}.

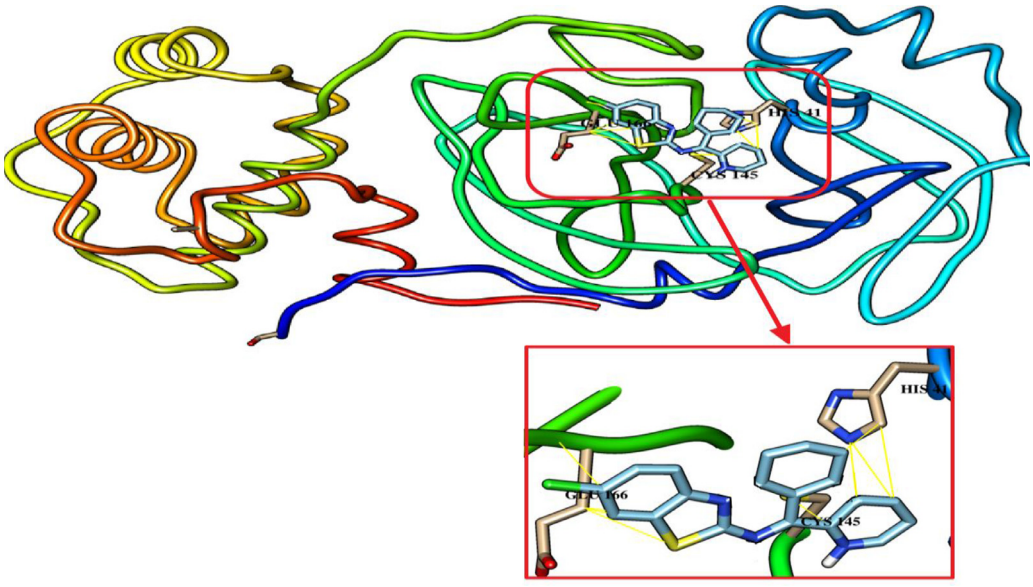

Fig. 9. **L³H** docked with 3-chymotrypsin-like protease (3CL^{pro}) of SARS-CoV-2. Hydrocarbon skeleton of **L³H** is cyan, nitrogen atoms are blue, oxygens red. Below, different side of view of magnified images of its contact sites to HIS^{41}, CYS^{145} and GLU^{166}.

Table 6
The binding interactions of **L¹H, L²H,** and **L³H** to 3-chymotrypsin-like protease of SARS-CoV-2.

Pharmaceutical name	Score (kcal/mol)	RMSD	Hydrogen bond (distance)	Van der Waal's (distance)
L¹H	-6.6	27.120 – 29.360	Glu^{166} (2.275 Å)	His^{41} (3.664 Å/ 3.777 Å). Cys^{145} (3.470 Å/ 3.490 Å). Glu^{166} (14 side contacts, distance range: 2.275 Å to 3.826Å).
L²H	-7.6	28.639 – 31.280	-	His^{41} (5 side contacts, distance range 3.464 Å to 3.785 Å). Cys^{145} (3.707 Å) Glu^{166} (6 side contacts, distance range 3.440 Å to 3.780 Å).
L³H	-7.6	1.524 - 6.174	-	His^{41} (4 side contacts, distance range 3.624 Å to 3.826 Å). Cys^{145} (3.779 Å) Glu^{166} (4 side contacts, distance range 3.390 Å to 3.955 Å).

2 virus. The inhibitory effect was investigated based on their interaction to the catalytic residues of His^{41} and Cys^{145}, the essential residues of Glu^{166} and Ser^{1} for maintaining CL^{pro} on the correct conformation [33]. The synthetic compounds have been docked with $3CL^{pro}$. They form hydrogen bonds (blue stripes) and Van der Waal's interactions (yellow stripes) as depicted in Figs. 7-9. **L^2H** and **L^3H** have shown the best binding affinity of -7.6 for both. Of them, **L^3H** had a better RMSD as presented it Table 6. the synthetic Schiff bases **L^1H** OPT has shown a tendency to form hydrogen bonds with the active residue of Glu^{166}. Whereas, they are all interact with others catalytic residues of of His^{41} and Cys^{145} of CL^{pro}. Our results suggest these compounds as a potent CL^{pro} inhibitors, particularly **L^3H** and thus could be used for the treatment of COVID-19 after a suitable in vitro and in vivo validation as well as clinical trials.

4. Conclusion

New Schiff bases, N'-(phenyl(pyridin-2-yl)methylene)isonicotinohydrazide (**L^1H**), N-(2-((phenyl(pyridin-2-yl)methylene) amino)ethyl)naphthalen-1-amine (**L^2H**), and N-(6-chlorobenzo[d] thiazol-2-yl)-1-phenyl-1-(pyridin-2-yl)methanimine (**L^3H**) were synthesized by condensation of 2-benzoylpyridine with three different amines and characterized by different physicochemical studies. The antimicrobial activities of all complexes were tested at three concentrations 50, 100 and 200 μg/mL, against five bacterial types. **L^3H** is more active for the tested bacteria compared with other Schiff bases (**L^1H**, and **L^2H**) and has highest effective against the tested bacteria *S. aureus, M. luteus, S. pyogenes, B. subtilis* with MIC values of 6.25, 25, 25, and 25μg/mL, respectively, whereas a less active against *E. coli*, with MIC value 100μg/mL. The **L^3H** compound is more active than the other Schiff bases because it has a (Cl and S) atoms in the structure, these atoms possibly via enhanced membrane transport into the cell or some other mode of action. The compounds have also been docked with 3CLpro. They have shown good interaction with the catalytic sites of 3CLpro, thus could be consider as a potent inhibitors and therapeutic agents for COVID-19 after suitable in vitro and in vivo validation as well as clinical trials. The molecular docking results were illustrated in terms of the DFT calculations. The results of the DFT showed that **L^3H** is the most lying HOMO and therefore it may be the best to serve as an electron donor. In addition, N4, N5 and N16 are the most electrophilic centers of **L^3H** and this may be due to the presence of the lone pair of electrons on these atoms. Finally, performing further in vitro and small animal models is very promising in vivo studies establishing solid experimental evidence of its activity as COVID-19 inhibitors.

Declaration of Competing Interest

The authors declare no conflict of interest.

Supplementary materials

Supplementary material associated with this article can be found, in the online version, at doi:10.1016/j.molstruc.2020.129454.

CRediT authorship contribution statement

Ahmed S.M. Al-Janabi: Supervision, Conceptualization, Methodology, Investigation, Writing - review & editing. **Amin O. Elzupir:** Writing - review & editing, Data curation, Formal analysis. **Tarek A. Yousef:** Methodology, Investigation, Software, Writing - review & editing.

References

[1] H. Nishiura, N.M. Linton, A.R. Akhmetzhanov, Serial interval of novel coronavirus (COVID-19) infections, Int. J. Infect. Dis. 93 (2020) 284–286.
[2] D. Zhou, P. Zhang, C. Bao, Y. Zhang, N. Zhu, Emerging understanding of etiology and epidemiology of the novel coronavirus (COVID-19) infection in Wuhan, China, Preprints (2020), doi:10.20944/preprints202002.0283.v1.
[3] N. Zhu, D. Zhang, W. Wang, X. Li, B. Yang, J. Song, X. Zhao, B. Huang, W. Shi, R. Lu, I China Novel Coronavirus, T. Research, A novel coronavirus from patients with pneumonia in China, 2019, Engl. J. Med. 382 (2020) 727–733.
[4] F. Cheng, In silico oncology drug repositioning and polypharmacology, in: Cancer Bioinformatics, Springer, Cham, Switzerland, 2019, pp. 243–261.
[5] C. Liu, Y. Ma, J. Zhao, R. Nussinov, Y.-C. Zhang, F. Cheng, Z.-K. Zhang, Computational network biology: data, model, and applications, Phys. Rep. 846 (2019) 1–66.
[6] S. Theerawatanasirikul, C.J. Kuo, N. Phetcharat, P. Lekcharoensuk, In silico and in vitro analysis of small molecules and natural compounds targeting the 3CL protease of feline infectious peritonitis virus, Antivir. Res. 174 (2020) 104697.
[7] M. Hagar, K. Chaieb, S. Parveen, H. Ahmed, R. Alnoman, N-alkyl 2-pyridone versus O-alkyl 2-pyridol: ultrasonic synthesis, DFT, docking studies and their antimicrobial evaluation, J. Mol. Struct. 1199 (2020) 126926.
[8] R.B. Alnoman, S. Parveen, M. Hagar, H.A. Ahmed, J.G. Knight, A new chiral boron–dipyrromethene (BODIPY)–based fluorescent probe: molecular docking, DFT, antibacterial and antioxidant approaches, J. Biomol. Struct. Dyn. 19 (2019) 1–14, doi:10.1080/07391102.2019.1701555.
[9] R.B. Alnoman, M. Hagar, S. Parveen, H.A. Ahmed, J.G. Knight, Computational and molecular docking approaches of a new axially chiral BODIPY fluorescent dye, J. Photochem. Photobiol. A: Chem. 395 (2020) 112508.
[10] K.S. Kumar, S. Ganguly, R. Veerasamy, E. De Clercq, Synthesis, antiviral activity and cytotoxicity evaluation of Schiff bases of some 2-phenyl quinazoline-4(3)H-ones, Eur. J. Med. Chem. 45 (11) (2010) 5474–5479.
[11] D. Chang, M. Lin, L. Wei, L. Xie, G. Zhu, C.S.D. Cruz, L. Sharma, Epidemiologic and clinical characteristics of novel coronavirus infections involving 13 patients outside Wuhan, China, JAMA 323 (11) (2020) 1092–1093.
[12] P. Zhou, H. Fan, T. Lan, X.L. Yang, W.F. Shi, W. Zhang, Y. Zhu, Y.W. Zhang, Q.M. Xie, S. Mani, X.S. Zheng, X.S., Fatal swine acute diarrhoea syndrome caused by an HKU2-related coronavirus of bat origin, Nature 556 (2020) (2018) 255–258.
[13] D. Benvenuto, M. Giovanetti, A. Ciccozzi, S. Spoto, S. Angeletti, M. Ciccozzi, The 2019-new coronavirus epidemic: evidence for virus evolution, J. Med. Vir. 92 (4) (2020) 455–459.
[14] A.W. Bauer, Single-disk antibiotic-sensitivity testing staphylococci, Arch. Internal Med. 104 (2) (1959) 208–216.
[15] P.R. Murray, E.J. Baron, M.A. Pfaller, F.C. Tenover, R.H. Yolken, G.L. Wood, J.A. Washington, Manual of clinical microbiology, Washington. DC. (1995).
[16] Gaussian 09Revision a. 02, gaussian. Inc., Wallingford, CT, USA, 2009.
[17] R.C. Edgar, B.J. Haas, J.C. Clemente, C. Quince, R. Knight, UCHIME improves sensitivity and speed of chimera detection, Bioinformatics 27 (16) (2011) 2194–2200.
[18] E.F. Pettersen, T.D. Goddard, C.C. Huang, G.S. Couch, D.M. Greenblatt, E.C. Meng, T.E. Ferrin, UCSF chimera—a visualization system for exploratory research and analysis, J. Comput. Chem. 25 (13) (2004) 1605–1612.
[19] O. Trott, A.J. Olson, Auto dock vina: improving the speed and accuracy of docking with a new scoring function, efficient optimization, and multithreading, J. Comput. Chem. 31 (2) (2010) 455–461.
[20] J. Devi, N. Batra, R. Malhotr, Ligational behavior of Schiff bases towards transition metal ion and metalation effect on their antibacterial activity, Spectrochimica Acta A 97 (2012) 397–405, doi:10.1016/j.saa.2012.06.026.
[21] O.A.M. Ali, S.M. El-Medani, D.A. Ahmed, D.A. Nassar, Synthesis, characterization, fluorescence and catalytic activity of some new complexes of unsymmetrical Schiff base of 2-pyridinecarboxaldehyde with 2,6-diaminopyridine, Spectrochimica Acta Part A 144 (2015) 99–106, doi:10.1016/j.saa.2015.02.078.
[22] R.M. Silverstein, F.X. Webster, Spectrometric Identification of Organic Compounds, 6th ed., John Wiley & Sons, New York, NY, USA, 1997.
[23] A.F. Tarek, A.S. Fayzah, B. Jubair, A.W. Omima, Schiff bases of indoline-2,3-dione (isatin) derivatives and nalidixicacidcarbohydrazide, synthesis, antitubercular activity and pharmacophoricmodelbuilding, Eur. J. Med. Chem. 45 (2010) 4578–4586.
[24] G. Küçükgüzel, S. Rollas, I. Küçükgüzel M. Kiraz, Synthesis and antimycobacterial activity of some coupling products from 4-aminobenzoic acid hydrazones, Eur. J. Med. Chem. 34 (12) (1999) 1093–1100.
[25] S.K. Sridhar, M. Saravanan, A. Ramesh, Synthesis and antibacterial screening of hydrazones, Schiff and MANNICH bases of isatin derivatives, Eur. J. Med. Chem. 36 (7-8) (2001) 615–625 (2001).
[26] N.V. Prabhu, K.A. Sharp, Heat capacity in proteins, Annu. Rev. Phys. Chem. 56 (2005) 521–548.
[27] 3R. Sato, S. Vohra, S. Yamamoto, K. Suzuki, K. Pavel, S. Shulga, Y. Blume, N. Kurita, Specific interactions between tauprotein and curcumin derivatives: molecular docking and abinitio molecular orbital simulations, J. Mol. Graph. Model. 98 (2020) 107611.
[28] D. Majumdar, D.K. Singh, D.K. Pandey, D. Parai, K. Bankura, D. Mishra, DFT investigations of linear Zn3-typecomplexwithcompartmentalN/O-donor Schiff base: synthesis, characterizations, crystal structure, fluorescence and molecular docking, J. Mol. Struct. 1209 (2020) 127936.
[29] M.S. Almutairi, D. Leenaraj, H.A. Ghabbour, I.H. Joe, M.I. Attia, Spectroscopic identification, structural features, hirshfeld surface analysis and molecular

docking studies on stiripentol: an orphan antiepileptic drug, J. Mol. Struct. 1180 (2019) 110–118.
[30] T.A. Yousef, G.M. Abu El-Reash, R.M. El Morshedy, Quantum chemical calculations, experimental investigations and DNA studies on (E)-2-((3-hydroxynaphthalen-2-yl) methylene)-N-(pyridin-2-yl) hydrazinecarbothio- amide and its Mn (II), Ni (II), Cu (II), Zn (II) and Cd (II) complexes, Polyhedron 45 (2012) 71–85.
[31] T.A. Yousef, O.K. Alduaij, G.M. Abu El-Reash, R.M. El Morshedy, Semiempirical studies, spectral analysis, in vitro antibacterial and DNA degradation studies of heterocyclic thiosemicarbazone ligand and its metal complexes, J. Mol. Liq. 222 (2016) 762–776.
[32] T.A. Yousef, Structural, optical, morphology characterization and DFT studies of nano sized Cu (II) complexes containing schiff base using green synthesis, J. Mol. Struct. 1215 (2020) 128180.
[33] L. Zhang, D. Lin, X. Sun, U. Curth, C. Drosten, L. Sauerhering, S. Becker, K. Rox, R. Hilgenfeld, Crystal structure of SARS-CoV-2 main protease provides a basis for design of improved α-ketoamide inhibitors, Science 368 (6489) (2020) 409–412.